International Journal of Mechanical Engineering (IJME)
ISSN(P): 2319-2240; ISSN(E): 2319-2259
Vol. 2, Issue 5, Nov 2013, 151-164

International Academy of Science, Engineering and Technology
Connecting Researchers; Nurturing Innovations

NUMERICAL INVESTIGATION ON HYDRODYNAMIC FIELD CHARACTERISTICS FOR TURBULENT FLOW OF WATER-TiO_2 NANOFLUID IN A CIRCULAR TUBE

M. S. YOUSSEF[1], ABDEL-FATTAH M. MAHROUS[2] & EL-SHAFEI B. ZEIDAN[3]

[1,2,3]Department of Mechanical Engineering, College of Engineering, Taif University, Al-Haweiah, Saudi Arabia

[1]Department of Mechanical Engineering, Faculty of Engineering, Assiut University, Assiut, Egypt

[2]Department of Mechanical Power Engineering, Faculty of Engineering, Shebin-ElKom University, Egypt

[3]Department of Mechanical Power Engineering, Faculty of Engineering, Mansoura University, Mansoura, Egypt

ABSTRACT

The hydrodynamic field characteristics of TiO_2-water nanofluid flowing in a circular tube under turbulent flow regime have been numerically investigated. A single phase fluid model in conjunction with two-equation turbulence model was employed in commercial soft ware package to determine the different turbulent quantities of nanofluid with different volume concentrations. Effects of nanoparticle volume concentrations on the turbulent quantities profiles of the hydrodynamic field are presented and discussed. The present study disclosed a novel features, for the first time to the author's knowledge; for the hydrodynamic characteristics of nanofluids. For example, with volume concentration $\varphi = 9$ % of TiO_2, the turbulent shear stress and turbulent kinetic energy were increased by 400 % of the base fluid, while, the turbulent eddy viscosity increased by 100 % and the dissipation rate of turbulent kinetic energy increased by 800 % of the base fluid. Moreover, the dimensionless constants κ and B in the well-known logarithmic velocity profile were found to be nanoparticle volume concentration dependents. Ultimately, in case of TiO_2-water nanofluid, the turbulent kinetic energy and shear stress have been revealed to satisfy the near-wall limiting behaviour similar to the base fluid. Further numerical studies focusing on other nanofluids are needed to judge the reported surprising simulated results.

KEYWORDS: Nanofluids, Numerical Simulation, Nanoparticle, Turbulent Flow, Laminar Flow

INTRODUCTION

Nanofluid, a term coined by Choi [1] of the Argonne National Laboratory, is a fluid including nanoparticles. This means that a "*nanofluid*" refers to a two-phase mixture with its continuous phase being generally a liquid and the dispersed phase constituted of fine particles. These suspended particles are extremely fine metallic particles of size below 100 nm and thus called "*nanoparticles*". The large surface-area-to-volume ratio increases the stability of the suspensions. For example, the thermal properties of such a nanofluid appear to be well above those of the base-fluid and, in particular, the suspended nanoparticles remarkably increase the thermal conductivity of the mixture and improve its capability of energy exchange. Thus, the nanofluid has become a new promising heat transfer fluid in a variety of application cases (see for example [2-4]). Nanoparticles used in nanofluids have been made out of many materials by physical or chemical processes [2]. Typical physical processes include the mechanical grinding method and the inert-gas –condensation technique. Chemical methods for producing nanoparticles include chemical precipitation, chemical vapor deposition, micro-emulsion, spray pyrolysis, and thermal spraying. In powder form, nanoparticles can be dispersed in aqueous or organic host liquids to form nanofluids for specific applications. Nanoparticle materials that have been used in nanofluid are oxide-, nitride-, carbide-, ceramics, metals, and semiconductors. Many types of host liquids have been used including ethylene glycol and water mixtures.

While thermal properties are important for heat transfer applications, the viscosity is also important because the pressure drop and the resulting pumping power depend on the viscosity. Therefore, many experimental and theoretical investigations focus on the heat transfer enhancement and pressure drop in various engineering applications. Various theoretical/numerical models were proposed to study the mechanism and predict the thermal conductivity and pressure drop of different nanofluids [5-14]. The numerical studies of nanofluids can be conducted using either single-phase (homogenous) or two-phase approaches. In the former approach it is assumed that the fluid phase and nanoparticles are in thermal equilibrium with zero relative velocity. While, in the latter approach, base fluid and nanoparticles are considered as two different liquid and solid phases with different momentums respectively [14]. Some of the published articles were related to investigation of laminar convective heat transfer of nanofluids [6, 11, 13], while, the others were concerning with turbulent ones [5, 7-10, 12].

Laminar forced convection of Al_2O_3-water nanofluid with 47 nm diameter flowing in the radial flow cooling system has been numerically simulated by Yang and Lai [6]. Their computational results using a single-phase approach revealed that the heat transfer coefficient increases with the increase of the Reynolds number and the nanoparticle volume fraction, though the increase in pressure drop was more significantly associated with the increase of particle concentration. Also, in another article for the same authors Yang and Lai [11], laminar forced convection flow of Al_2O_3-water nanofluid of 47 nm diameter in a radial flow cooling system using a single-phase approach has been simulated. Their simulated results confirmed that the Nusselt number increases with the increase of the Reynolds number and the nanoparticle volume fraction, though the increase in pressure drop is more significant with the increase of particle concentration. Fard et al. [13] used Computational Fluid Dynamics (CFD) approach based on single-phase and two-phase models to study laminar convective heat transfer of nanofluids with different volume concentration in a circular tube. Their numerical results have clearly shown that nanofluids with higher volume concentration have higher heat transfer coefficient and pressure drop. Moreover, their results revealed that, two-phase model showed better agreement with experimental data.

Turbulent flow and heat transfer of three different nanofluids flowing through a circular tube under constant heat flux condition have been numerically analyzed by Namburu et al. [5]. They assumed and used single-phase fluid model to solve two-dimensional steady, forced turbulent convection flow of nanofluid flowing inside a straight circular tube. Two-equation turbulence model of launder and Spalding was adopted by Namburu et al. [5] in their numerical analysis. Their computed results indicated that heat transfer coefficient and pressure loss increase with increase in the volume concentration of nanofluids and Reynolds number. An Eulerian-Lagrangian based direct numerical simulation model was developed by Kondaraju et al. [7] to investigate the effective thermal conductivity of nanofluids. Two different nanofluids namely Cu/water and Al_2O_3/water with different nanoparticles, 100 nm and 80 nm, respectively were simulated at different volume fractions. Numerical model of Kondaraju et al. [7] achieved a good comparison of the calculated effective thermal conductivity values with that of the experimental data. Also, the numerical calculated results show an increase in the thermal conductivity of nanofluids with the increase of volume fraction. Turbulent forced convection flow of a nanofluid that consists of water and Al_2O_3 (with average diameter of 42 nm) in horizontal tubes has been studied numerically by Lotfi et al. [8]. A single-phase model and two-phase mixture model formulations were used in their numerical study. The comparison of calculated results with experimental values shows that the mixture model was more precise and also the rate of thermal enhancement decreases with the increase of nanoparticles volume concentration. Steady state turbulent forced convection flow of water-Al_2O_3 nanofluid in a circular tube was numerically analyzed by Bianco et al. [9]. In their analysis, two different approaches were taken into consideration, single and two-phase models, and nanoparticle diameter equal to 38 nm has been used. It was observed from the numerical results that heat transfer enhancement increases with the

particle volume concentration and Reynolds number. Commercial CFD package, FLUENT, was used by Demir et al. [10] for solving the volume-averaged continuity, momentum, and energy equations of water with TiO_2 and Al_2O_3 nanofluids flowing in a horizontal tube under constant temperature condition. Their numerical results have clearly indicated that nanofluids with higher volume concentration have higher heat transfer enhancement and also have higher pressure drop. The reason for increasing the pressure drop is attributed to increasing velocity and viscosity of nanofluid. Meibodi et al. [12] used friction factor and convection coefficient in order to compare both velocity and temperature profiles for nanofluids and base fluids. They selected Al_2O_3/water and carbon nanotube/water as nanofluids. Meibodi and his co-workers' results show that velocity profile of a nanofluid was similar to the velocity profile of its base fluid.

To summarize what is reviewed above, in both laminar and turbulent flow regimes studied, almost all articles have focused on the heat transfer enhancement in terms of heat transfer coefficient or Nusselt number. Some articles have paid special attention to not only heat transfer enhancement but also the pressure drop of nanofluids flow or correspondingly the pumping power losses. Since the heat transfer coefficient value is affected by velocity and temperature profiles [12], therefore, understating the physics of the hydrodynamic field of nanofluid is indispensable not only in laminar regime but also in case of turbulent regime. It is well known to the authors' knowledge that; the hydrodynamic field of nanofluids in turbulent flow regimes has not been reported yet. As a result, this proposal aims at numerically studying the flow field characteristics of nanofluids in a circular tube under turbulent flow regimes using a single-phase approach in conjunction with two-equation turbulence model to determine the turbulent quantities. The effects of nanoparticles volume concentrations on the flow field characteristics are examined. The different turbulent quantities of hydrodynamic field are calculated and compared with the available of experimental data reported in the literature.

PHYSICAL PROPERTIES OF NANOFLUIDS

The physical properties of nanofluids are vital in simulation process because the results are strongly affected by them. The following formulas have been employed to compute the physical properties of nanofluids under consideration. The densities of nanofluids have been estimated using the classical formula developed for conventional solid-liquid mixtures (see for example, Bianco et al. [9] and, Yang and Lai [11]):

$$\rho_{nf} = (1-\varphi)\,\rho_{bf} + \varphi\,\rho_P \tag{1}$$

Where φ denotes the volume concentration of nanoparticles. The subscripts nf, bf, and P refer to the nanofluid, base fluid (water), and nanoparticles, respectively. It must be mentioned that, Eq. (1) satisfies the mass continuity if volume of suspension is equated to the sum of volume of fluid and volume of particles.

Regarding the dynamic viscosity of nanofluids, many proposals have been reported in the literature review; such as Brinkman [15], Drew and Passman [16], Bastchelor [17], and Wang et al. [18]. In the present study, the following formula proposed by Wang et al. [18] is used to predict the dynamic viscosity of nanofluids.

$$\mu_{nf} = (1 + 7.3\varphi + 123\varphi^2)\mu_{bf} \tag{2}$$

The tabulated values for the density and dynamic viscosity of the base fluid (water) are fitted in polynomial functions of temperature (in Kelvin) using Engineering Equation Solver (EES) and are written in the following forms:

$$\rho_{bf} = 2813.77 \times 10^{-1} + 6351.93 \times 10^{-3}\,\mathrm{T} - 1761.03 \times 10^{-5}\,T^2 + 1460.96 \times 10^{-8}\,T^3 \tag{3}$$

$$\mu_{bf} = 9684.22 \times 10^{-5} - 821.53 \times 10^{-6}\,\mathrm{T} + 2345.21 \times 10^{-9}\,T^2 - 2244.12 \times 10^{-12}\,T^3 \tag{4}$$

These properties were used as user defined functions (UDF) subroutines and incorporated into FLUENT 6.3 solver [19].

MODELING APPROACH

Assumption

It is assumed that the fluid phase and nanoparticles are in thermal equilibrium with zero relative velocity. This assumption may be considered realistic as nanoparticles are much smaller than microplarticles and the relative velocity decreases as the particle size decreases. Thus, the resultant mixture may be considered as a conventional single phase fluid [5]. Figure 1 shows the considered geometrical configuration of the computational domain. It consists of a tube with length of 1.8 m and circular section with internal diameter of 0.008 m. The considered nanofluid is a mixture composed of water and particles of TiO_2. The flow field is assumed to be axisymmetric with respect to the horizontal plane parallel to the tube axis.

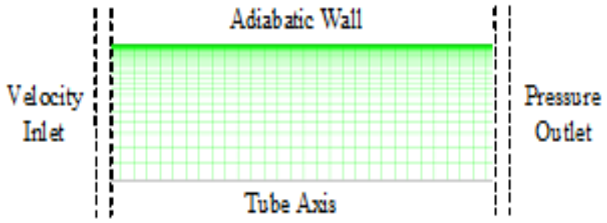

Figure 1: Schematic of the Configuration of Computational Domain

Governing Equations

The problem under study is a two-dimensional axisymmetric, incompressible, and steady flow of water-TiO_2 nanofluid flowing inside a straight circular tube having diameter of 0.008 m and length of 1.8 m. The flow has been modelled using Navier-Stokes equations solved by FLUENT 6.3 solver [19]. The single-phase homogeneous flow continuity and momentum equations in Cartesian coordinates are respectively written (see for example Nagano and Tagawa [20]) as:

$$\frac{\partial}{\partial x_i}(\bar{U}_i) = 0 \tag{5}$$

$$\frac{D\bar{U}_i}{D\tau} = -\frac{1}{\rho}\frac{\partial \bar{P}}{\partial x_i} + \frac{\partial}{\partial x_j}\left(\nu\frac{\partial \bar{U}_i}{\partial x_j}\right) - \frac{\partial}{\partial x_j}\left(\overline{u_i u_j}\right) \tag{6}$$

Where the substantial derivative $D/D\tau = \partial/\partial\tau + \bar{U}_j\,\partial/\partial x_j$, ρ is the fluid density, $\bar{U}_i$ is the mean velocity component in x_i direction, u_i is the fluctuating velocity component in x_i direction, ν is the kinematic viscosity, and $\bar{P}$ is the static pressure. The turbulent shear stress in Eq. (6) is unknown and must be calculated via a turbulence model.

Turbulence Modeling

In order to determine the characteristics of the hydrodynamic field, it is necessary to close the governing equations (Eqs. 5 & 6). To do so, $k-\varepsilon$ eddy viscosity model proposed by Shih et al. [21] is employed to determine the turbulent shear stress and correspondingly Eqs. (5) & (6) are closed. Shih and his co-workers used a realizable Reynolds stress algebraic model which its linear form represents an isotropic eddy viscosity model as follows:

$$-\overline{u_i u_j} = \nu_t\left(\frac{\partial \bar{U}_i}{\partial x_j} + \frac{\partial \bar{U}_j}{\partial x_i}\right) - \frac{2}{3}\,\mathrm{k}\,\delta_{\mathrm{ij}} \tag{7}$$

$$\nu_t = C_\mu\frac{k^2}{\varepsilon} \tag{8}$$

Here the coefficient C_μ is not a constant as in the standard $k-\varepsilon$ turbulent model but takes the following formulation:

$$C_\mu = \frac{1}{4+A_S U^{(*)}\frac{k}{\varepsilon}} \tag{9}$$

Details about the parameters A_s and $U^{(*)}$ are given in the article of Shih et al. [21].

The turbulent kinetic energy, k, and its dissipation rate, ε, in Eq. (8) are determined from additional two differential equations as follows [21]:

$$\frac{Dk}{D\tau} = \frac{\partial}{\partial x_j}\left\{\frac{\nu_t}{\sigma_k}\frac{\partial k}{\partial x_j}\right\} - \overline{u_i u_j}\frac{\partial \bar{U}_i}{\partial x_j} - \varepsilon \tag{10}$$

$$\frac{D\varepsilon}{D\tau} = \frac{\partial}{\partial x_j}\left\{\frac{\nu_t}{\sigma_\varepsilon}\frac{\partial \varepsilon}{\partial x_j}\right\} - C_1 S\,\varepsilon - C_2\frac{\varepsilon^2}{k+\sqrt{\nu\varepsilon}} \tag{11}$$

The different constants in Eqs. (10) and (11) are $C_2 = 1.9$; $\sigma_k = 1.0$, and $\sigma_\varepsilon = 1.2$, while, the coefficient C_1 is given as follows:

$$C_1 = \max\left\{0.43, \frac{\eta}{5+\eta}\right\},\ \eta = \frac{Sk}{\varepsilon}, S = \sqrt{2S_{ij}S_{ij}}\ , S_{ij} = \frac{1}{2}\left(\frac{\partial \bar{U}_i}{\partial x_j} + \frac{\partial \bar{U}_j}{\partial x_i}\right) \tag{12}$$

Further information about the turbulence model used in this study is available in Shih et al. [21] and FLUENT 6.3 solver [19].

Boundary Conditions and Grid System

The governing equations of the fluid flow are nonlinear and coupled partial differential equations. Inlet velocity and pressure outlet boundary conditions were, respectively, imposed at the inlet and outlet sections of the tube. No-slip conditions for velocity components and zero normal pressure gradients were set as the boundary conditions for solid wall. The boundary values for the turbulent quantities near the wall are specified using the two layers enhanced wall treatment functions [19]. It must be mentioned here that, only half of the tube was modelled due to the symmetry.

In order to ensure fully developed turbulent flow at the entry of the tube section, an additional tube length of 0.3 m is modelled along with the main tube length of 1.5 m. The computational domain was discretized using structured non-uniform rectangular cells. By employing a nonuni form grids scheme, as shown in Figure 1, the mesh density near the wall is about five times that of the mesh density at the centre of the tube. Following a grid-independence solution test, the computational grid has an average mesh density of about 20 cells/mm^2.

Numerical Method

The conservation equations of mass, momentum, turbulent kinetic energy, and dissipation rate of turbulence, Eqs. (5), (6), (10), and (11), respectively, were solved by control volume approach. Control-volume technique converts the conservation equations to a set of linear algebraic equations that can be solved numerically. A second order upwind descritization scheme was used to interpolate the unknown cell interface values required for the modelling of convection terms. Coupling between velocity and pressure was resolved by using Semi Implicit Method for Pressure Linked Equations [SIMPLE] algorithm [22]. FLUENT 6.3 code solves the linear systems resulting from discretization schemes. During the iteration process, the residuals were carefully monitored and converged solutions were considered when the following criterion for convergence is satisfied:

$$\max\left|\frac{\theta^{i+1}}{\theta^{i}}-1\right|<10^{-7} \tag{12}$$

Where θ: $\overline{U}$, k, and ε and i denotes the number of iterations.

RESULTS AND DISCUSSIONS

Validation of the Present Computational Model

In order to verify the validity of the present computational model, the numerical results were compared with both theoretical data and experimental measurements available for the conventional fluids. For this purpose, the results of the experimental friction factor of pure water carried out by Duang thongsuk and Wong wises [23] have been used for comparison. The different quantities such as the average velocity, turbulent kinetic energy, and turbulent viscosity measured by Laufer [24] were also included in these comparisons. Regarding the theoretical calculation of friction factor, the Darcy friction factor,f, given by Blasius is presented as follows [5]:

$$f=0.3164\,Re^{-0.25} \tag{13}$$

Also, the friction factor can be calculated from Colebrook equation, cited in Duangthongsuk and Wongwises [23, 25], which is defined as follows:

$$\frac{1}{\sqrt{f}}=-2.0\log\left(\frac{\gamma/D}{3.7}+\frac{2.51}{Re\sqrt{f}}\right) \tag{14}$$

Where γ is the roughness of the test tube wall, D is the diameter of test tube, and Re is the Reynolds number of flow inside the test tube. Also, the predictions by Nagano and Tagaw' model were used to validate the present computational model. In the present study, the friction factor, *f*, was calculated according to Darcy-Weisbach Equation as:

$$f=-\frac{dP}{dz}\,\frac{2D}{\rho\overline{U}^{2}} \tag{15}$$

Where $\frac{dP}{dz}$ is the axial pressure gradient, *D* is the pipe diameter, and $\overline{U}$ is the average flow velocity. Therefore, for friction factor, *f*, of pure water, comparison will be made between the present output computational results from Eq. (15) with the calculated values from Eqs. (13) and (14) as well as the experimental data of Duangthongsuk and Wongwises [23]. It is seen from Figure 2, over the range of Reynolds numbers studied, an excellent agreement is observed between the simulated results and the experimental data, while, the computed values from theoretical Eqs. (13) & (14) give the same trend in accord with the experimental date. The simulated results of the normalized turbulent kinetic energy are compared with the experimental data of Laufer [24] and are shown in Figure 3. With the exception of peak value, the simulated results of turbulent kinetic energy are in excellent agreement with the experimental data. In order to explore more cases of validations, further comparisons for the average velocity and turbulent viscosity are carried out to convince the suitability of the present computational model. The simulated mean velocity field is compared with the experimental data of Laufer [24] and is shown in Figure 3. The general agreement is excellently in accord with the experimental data and with the well-known logarithmic velocity profile that is given as follows:

$$\overline{U}^{+}=\frac{1}{\kappa}\ln y^{+}+B \tag{16}$$

Where κ is Von Kármán constant and has a value of 0.4 and B = 5.5 [20]. As a final test case to confirm the accuracy of the present computational model, a comparisons of the simulated results of turbulent viscosity distributions and the calculated results obtained from Nagano and Tagawa' model along with experimental data of Laufer [24] are shown in Figure 5. Little discrepancy between both the present simulations and the calculated results of Nagano and

Tagawa' model in accord with the experimental data in the core region of the flow is noticed in Figure 5. This discrepancy is known as a common drawback of the $k-\varepsilon$ turbulent models as pointed by Nagano and Tagawa [20].

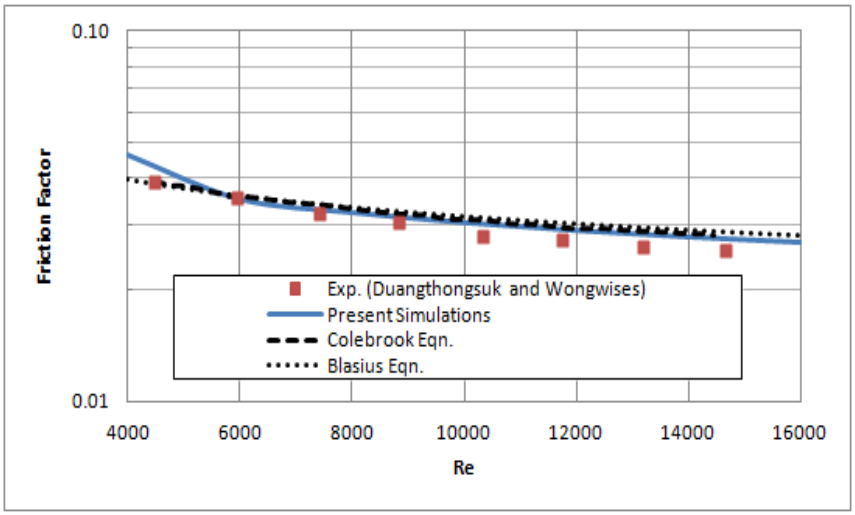

Figure 2: Friction Factor Distributions of Pure Water at Different Values of Reynolds Number in a Pipe

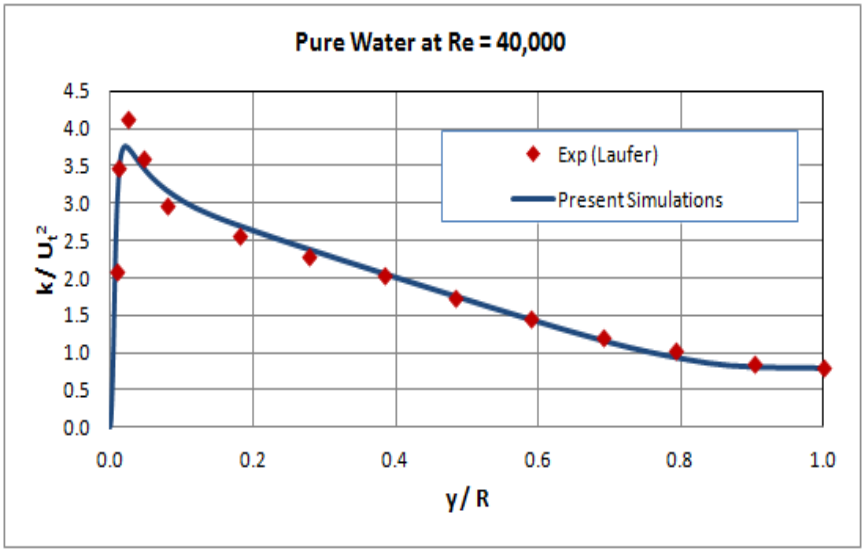

Figure 3: Turbulent Energy Profiles of Pure Water at Re = 40,000 in a Pipe

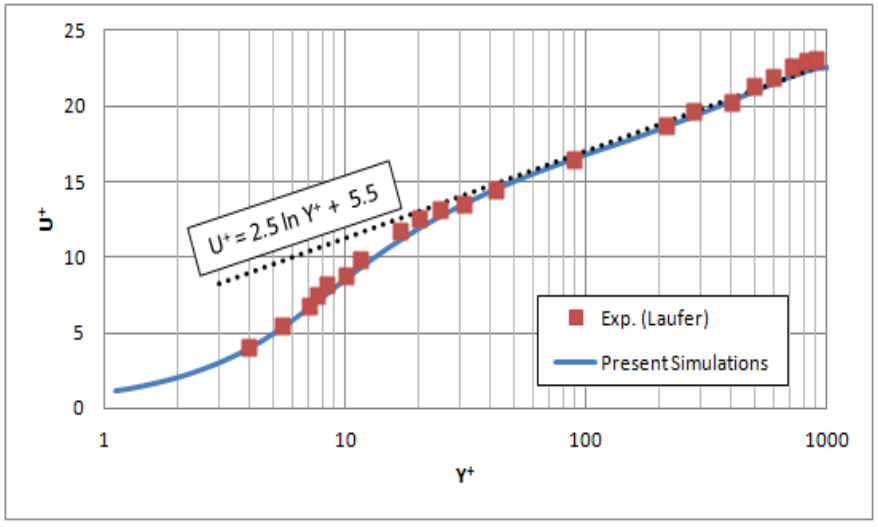

Figure 4: Mean Velocity Profiles of Pure Water at Re = 40,000 in a Pipe

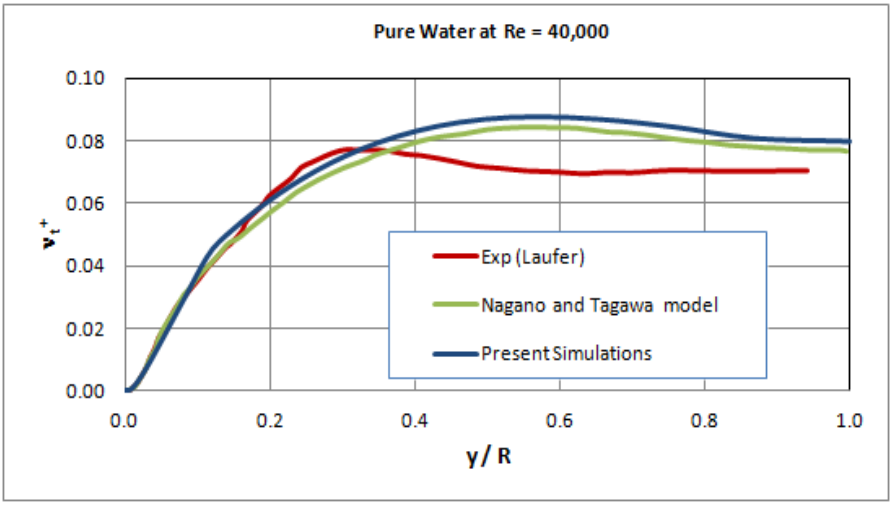

Figure 5: Turbulent Viscosity Distributions of Pure Water at Re = 40,000 in a Pipe

Application of the Present Computational Model

After the above four comparisons and confirming that the present computational model is generating correct results in case of pure water, nanofluids with varying volume concentrations are analyzed at the same value of Reynolds number of 40,000. The simulated results of mean velocity profiles at different values of volumetric concentrations, φ, ranging from 0 % (pure water) to 9 % are shown in Figure 6. As no experimental data, for the authors' knowledge, is available for the mean velocity at any value of volumetric concentration, we compared our results with the theoretical linear profile applied in viscous sublayer, $\bar{U}^+ = y^+$, and the logarithmic law profile mentioned in Eq. (16) applied in overlap layer. It must be mentioned here that, in a turbulent pipe flow, there is an overlap layer or intermediate region between the viscous and outer layers where both laminar and turbulent shear are important. Therefore, Figure 6 displays the influence of TiO_2 nanoparticle volume concentration, φ, on the average velocity. By increasing φ, the thickness of overlap layer increases and that is owing to the increase of viscosity of nanofluid. Moreover, the constant κ in Eq. (16) decreases by increasing the nanoparticle volume concentration which κ = 0.187 at φ = 9 %, while the constant B increases to have a value of 9.8 at φ = 9 %. Ultimately, the increase in average velocity is about 100 % with φ = 9 % over the base fluid at the studied Reynolds number of flow. Figures 7 & 8 show the near-wall and all domain behaviours of the turbulent kinetic energy, respectively, in a pipe flow at Reynolds number of 40,000 at different values of volume concentrations.

It is clear that the simulated results of the nanofluid at all values of the volume concentrations satisfy the limiting behaviour of wall turbulence of turbulent kinetic energy $k^+\alpha\ (y^+)^2$ as shown in Figure 7 and that is similar to single phase fluid as pointed out by Youssef [26 & 27]. The influence of TiO_2 nanoparticle volume concentration on the distributions of turbulent kinetic energy in pipe flow at Re = 40,000 is shown in Figure 8. The increase in the values of turbulent kinetic energy reaches about 400 % at φ = 9 % over the base fluid and that is reflected on the simulated results on Figures 9 & 10. The near-wall and all domain behaviours of the dissipation rate of turbulent kinetic energy, respectively, in a pipe flow at Reynolds numbers of 40,000 at different values of volume concentrations are shown in Figures 9 & 10. What has to be noticed from both figures is that the increase in the values of turbulent kinetic energy dissipation rate reaches about 800 % at φ = 9 % over the value of base fluid. A more evidence for these observations can be also depicted from the budget of turbulent kinetic energy and that is shown in Figure 11. In this figure, at the wall the viscous dissipation rate equals the dissipation rate, while, the production rate is almost balanced by the dissipation rate for $y^+ > 100$. Nevertheless, the same trend is observed for base fluid, not shown here, but quantitatively is different for the nanofluid studied in the present study. Figure 12 displays the simulated results for the turbulent eddy viscosity at different values of volumetric

concentrations φ. By increasing the values of φ, the turbulent eddy viscosity of nanofluid increases by 100 % over the base fluid value.

This means that, the turbulent shear stress increases by increasing the value of φ and that is correspondingly widen the thickness of the overlap layer as noticed in Figure 6. What we have seen in Figure 12 is explicitly reflected on Figure 13 where displays the Reynolds shear stress distributions in a pipe flow at Re = 40,000. It is clear from Figure 13 that the simulated results for the Reynolds shear stress exhibits an increase of its value to about 400 % of the base fluid value. This increase not only owing to the increase in turbulent kinetic energy and its dissipation rate as mentioned in Eq. (9). The turbulent shear stress of TiO_2-water nanofluid satisfies the near-wall limiting behaviour condition in which $+\overline{uv}^+\alpha\ (y^+)^3$ as pointed out by Youssef [26, 27].

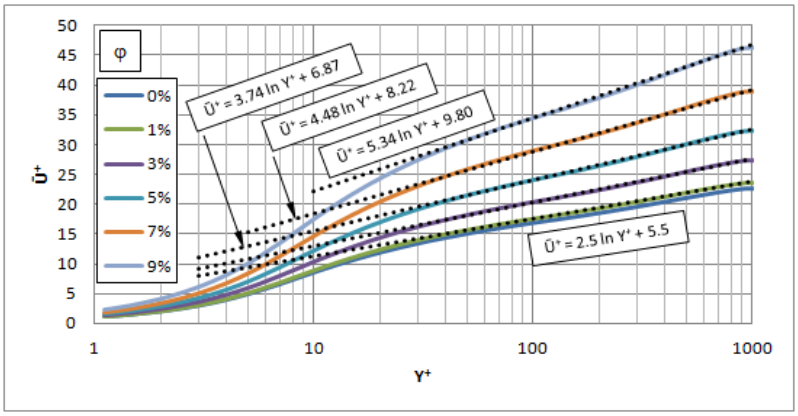

Figure 6: Mean Velocity Profiles in a Pipe Flow at Re = 40,000 at Different Values of φ

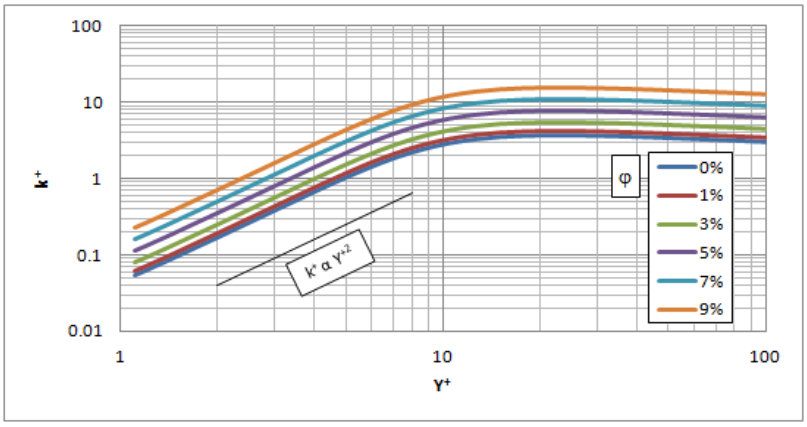

Figure 7: Near-Wall Distributions of Turbulent Kinetic Energy at Re = 40,000 at Different Values of φ

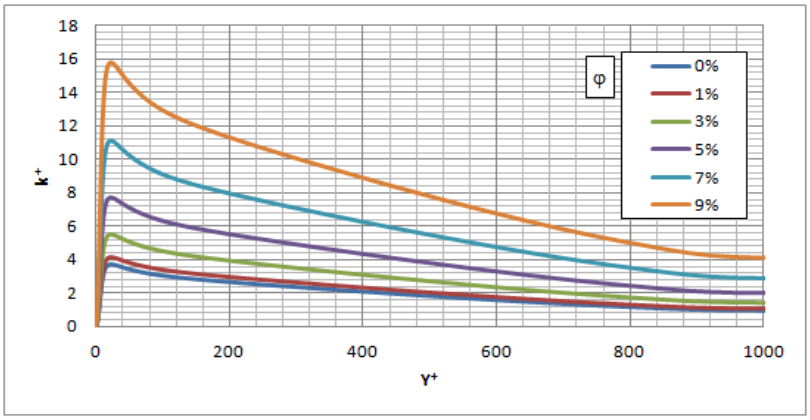

Figure 8: Distributions of Turbulent Kinetic Energy at Re = 40,000 at Different Values of φ

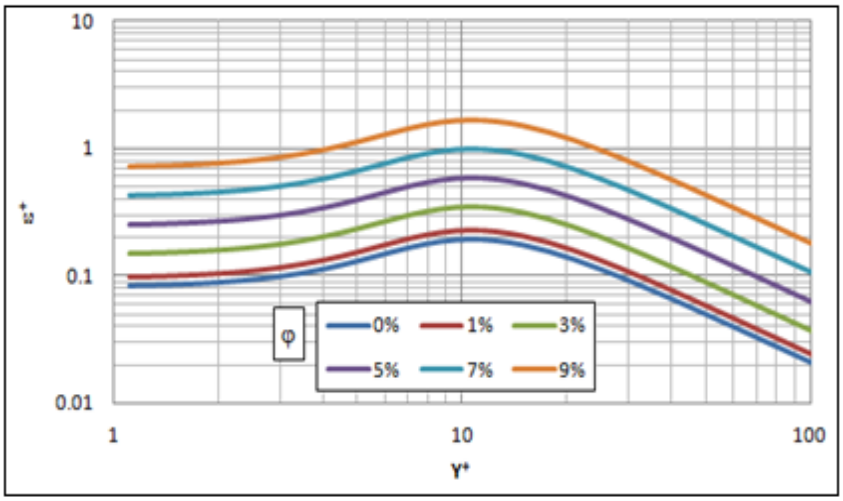

Figure 9: Near-Wall Distributions of Dissipation Rate of Turbulent Kinetic Energy at Re = 40,000 at Different Values of φ

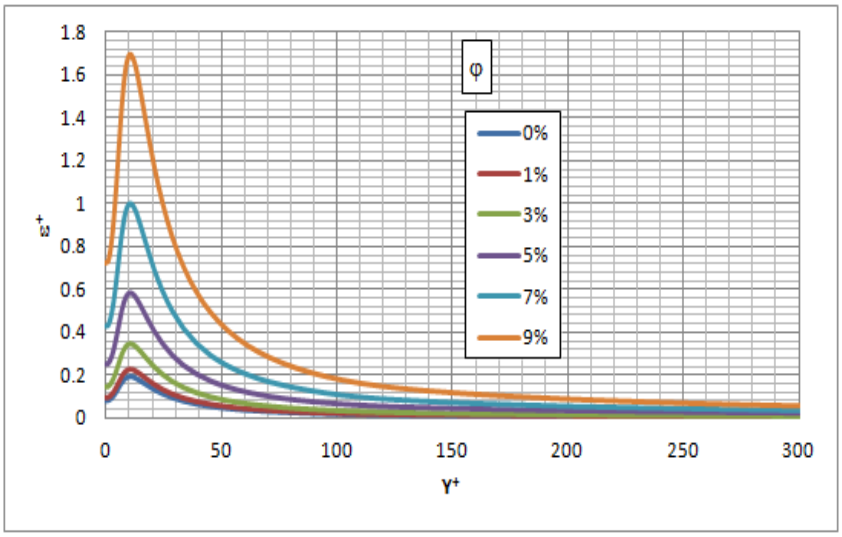

Figure 10: Distributions of Dissipation Rate of Turbulent Kinetic Energy at Re = 40,000 at Different Values of φ

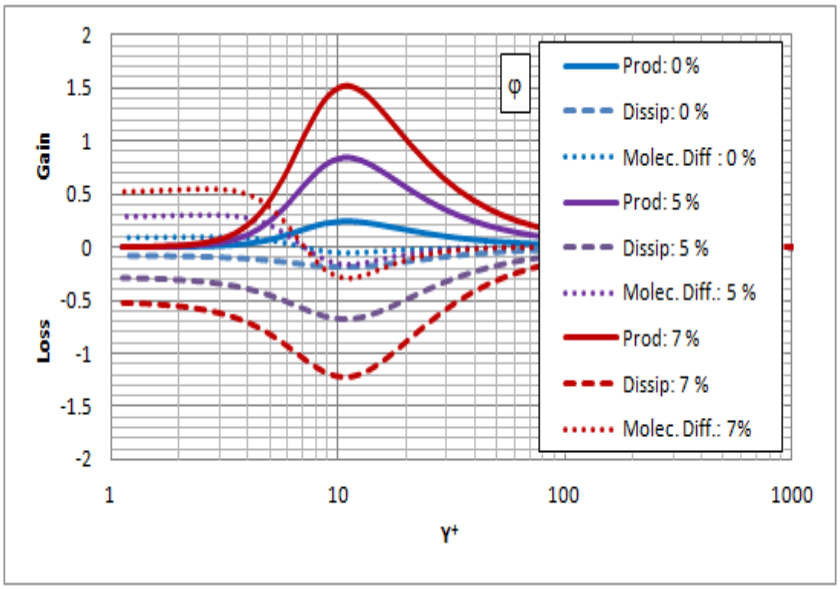

Figure 11: Budget of Turbulence Kinetic Energy in Pipe Flow at Re = 40,000 at Different Values of φ

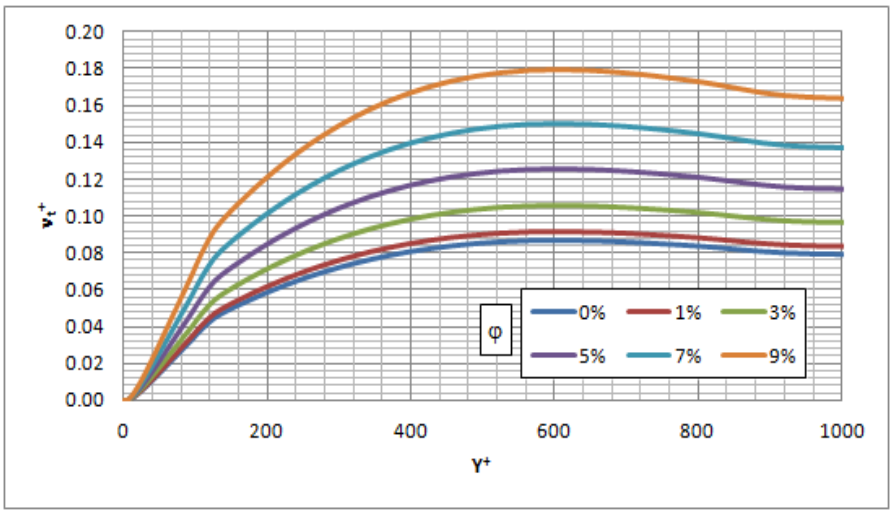

Figure 12: Distributions of Turbulent Eddy Viscosity in Pipe Flow at Re = 40,000 at Different Values of φ

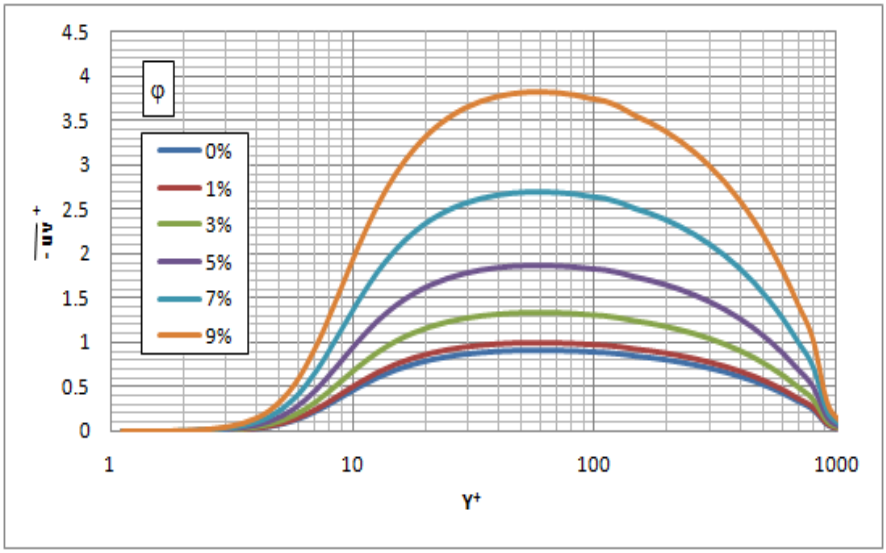

Figure 13: Reynolds Shear Stress Distributions in a Pipe Flow at Re = 40,000 at Different Values of φ

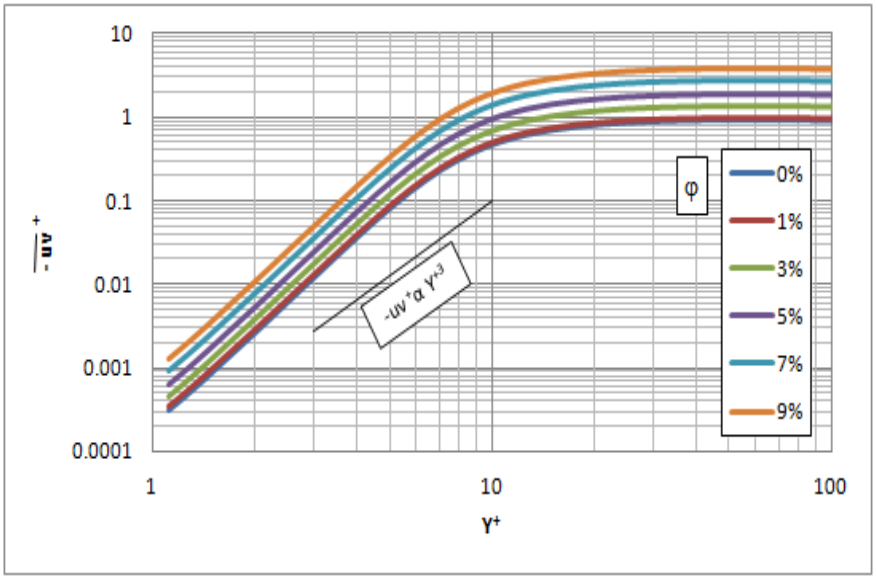

Figure 14: Near-Wall Distributions of Reynolds Shear Stress in a Pipe Flow at Re = 40,000

CONCLUSIONS

In this study, the hydrodynamic field characteristics of TiO_2-water nanofluid flowing in a circular tube under turbulent flow regime were numerically studied. A single phase fluid model in conjunction with two-equation turbulence model was employed in commercial soft ware package to determine the different turbulent quantities of nanofluid with different volume concentrations. It was revealed from the simulated results that by increasing TiO_2 nanoparticle volume concentration the different turbulent quantities increase to different values than the base fluid. For example, with volume concentration φ = 9 %, the turbulent shear stress and turbulent kinetic energy were increased by 400 % of the base fluid, while, the turbulent eddy viscosity increased by 100 % and the dissipation rate of turbulent kinetic energy increased by 800 % of the base fluid. Moreover, the dimensionless constants κ and B in the well-known logarithmic velocity profile were found to be nanoparticle volume concentration dependents. Ultimately, in case of TiO_2-water nanofluid, the turbulent kinetic energy and shear stress have been revealed to satisfy the near-wall limiting behaviour similar to the base fluid.

REFERENCES

1. S. U. S. Choi, "Enhancing thermal conductivity of fluids with nanoparticles," *in Developments Applications of Non-Newtonian Flows, D. A. Siginer and H. P. Wang, Eds., FED-Vol. 231/MD-Vol. 66, pp. 99-103, ASME, New York, NY, USA, 1995.*
2. W. Yu, D. M. France, J. L. Routbort, S. U. S. Choi, " Review and Comparison of Nanofluid Thermal Conductivity and Heat Transfer Enhancements," *Heat Transfer Engineering, Vol. 29(5), pp. 432-460, 2008.*
3. S. M. S. Murshed, K. C. Leong, C. Yang, Enhanced thermal conductivity of TiO_2-water based nanofluids," *International Journal of Thermal Sciences, Vol. 44 (4), pp. 706-714, 2009.*
4. J. J. Wang, R. T. Zheng, J. W. Gao, G. Chen, "Heat conduction mechanisms in nanofluids and suspensions," *Nano Today, Vol. 7 (2), pp. 124-126, 2012.*
5. P. K. Namburu, D. K. Das, K. M. Tanguturi, and R. S. Vajjha "Numerical study of turbulent flow and heat transfer characteristics of nano fluids considering variable properties," *International Journal of Thermal Sciences, Vol. 48, pp. 290-302, 2009.*
6. Y. T. Yang, and F. H. Lai "Numerical study of heat transfer enhancement with the use of nanofluids in radial flow cooling system," *International Journal of Heat and Mass Transfer, Vol. 53, pp. 5895-5904, 2010.*
7. S. Kondaraju, E. K. Jin, and J. S. Lee "Direct numerical simulation of thermal conductivity of nanofluids: The effect of temperature two-way coupling and coagulation of particles," *International Journal of Heat and Mass Transfer, Vol. 53, pp. 862-869, 2010.*
8. R. Lotfi, Y. Saboohi, and A. M. Rashidi "Numerical study of forced convective heat transfer of nanofluids: Comparison of different approaches," *International Communications in Heat and Mass Transfer, Vol. 37, pp. 74-78, 2010.*
9. V. Bianco, O. Manca, and S. Nardini "Numerical investigation on nanofluids turbulent convection heat transfer inside a circular tube," *International Journal of Thermal Sciences, Vol. 50, pp. 341-349, 2011.*
10. H. Demir, A. S. Dalkilic, N. A. Kürekci, W. Duangthongsuk, and S. Wongwises "Numerical investigation on the single phase forced convection heat transfer characteristics of TiO_2 nanofluids in a double-tube counter flow heat exchanger," *International Communications in Heat and Mass Transfer, Vol. 38, pp. 218-228, 2011.*

11. Y. T. Yang, and F. H. Lai "Numerical investigation of cooling performance with the use of Al_2O_3/water nanofluids in a radial flow system," *International Journal of Thermal Sciences, Vol. 50, pp. 61-72, 2011.*
12. T. P. Teng, Y. H. Hung, C. S. Jwo, C. C. Chen, and L. Y. Jeng "Pressure drop of TiO_2 nanofluid in circular pipes," *Particuology, Vol. 9, pp. 486-491, 2011.*
13. M. E. Meibodi, M. V. Sefti, A. M. Rashidi, A. Amrollahi, M. Tabasi, and H. S. Kalal "An estimation for velocity and temperature profiles of nanofluids in fully developed turbulent flow conditions," *International Communications in Heat and Mass Transfer, Vol. 37, pp. 895-900, 2010.*
14. M. H. Fard, M. N. Esfahany, and M. R. Talaie "Numerical study of convective heat transfer of nanofluids in a circular tube two-phase model versus single-phase model," *International Communications in Heat and Mass Transfer, Vol. 37, pp. 91-97, 2010.*
15. H. C. Brinkman"The viscosity of concentrated suspensions and solution", *Journal of Chemical Physics, Vol. 20, pp. 571-5xx, 1952.*
16. D. A. Drew, and S. L. Passman *"Theory of Multi-Component fluids"*, Springer, Berlin, 1999.
17. G. K. Batchelor "The effect of Brownian motion on the bulk stress in a suspension of spherical particles", *Journal of Fluid Mechanics, Vol. 83, No. 1, pp. 97-xx, 1977.*
18. X. Wang, X. Xu, S. U. S. Choi " Thermal conductivity of nanoparticles-fluid mixture", *Journal of Thermophysics of Heat Transfer, Vol. 13, No. 4, pp. 474-xx, 1999.*
19. FLUENT 6.3 user guide, Fluent Inc., Lebanon, New Hampshire, 2005.
20. Y. Nagano and M. Tagawa "An improved k-ε model for boundary layer flows", *ASME Journal of Fluids Engineering, Vol. 112, pp. 33-39, 1990.*
21. T.-H. Shih, W. W. Liou, A. Shabbir, Z. Yang, and J. Zhu "A new k − ε eddy viscosity model for high Reynolds number turbulent flows- Model development and validation", *NASA Technical Memorandum 106721, ICOMP-94-21; CMOTT-94-6.*
22. S. V. Patankar *"Numerical Heat Transfer and Fluid Flow"*, Hemisphere Publishing Corporation, New York, 1980.
23. W. Duangthongsuk and S. Wongwises "An experimental study on the heat transfer performance and pressure drop of TiO_2-water nanofluids flowing under a turbulent flow regime," *International Journal of Heat and Mass Transfer, Vol. 53, pp. 334–344, 2010.*
24. J. Laufer, "The structure of turbulence in fully developed pipe flow", NACA Report, Report number 1174, 1954.
25. W. Duangthongsuk and S. Wongwises "Heat transfer enhancement and pressure drop characteristics of TiO_2-water nanofluid in a double-tube counter flow heat exchanger", *International Journal of Heat and Mass Transfer, Vol. 52, pp. 2059–2067, 2009.*
26. M. S. Youssef " Prediction of channel flows with a low-Reynolds-number $k - k\tau$ Turbulence model", *Journal of Engineering Sciences, Assiut University, Vol. 32, No. 2, pp. 819-836, April 2004.*

27. M. S. Youssef "A two-equation heat transfer model for wall turbulent shear flows", *Journal of Engineering Sciences, Assiut University, Vol. 34, No. 6, pp. 1877-1903, November 2006.*

APPENDICES

Nomenclature

	Roman Symbols
C_1, C_2, C_μ	Turbulence model coefficients
D	Pipe diameter
f	Friction factor
k	Turbulent kinetic energy
$\bar{P}$	Average pressure
R	Pipe radius
Re	Reynolds number
S_{ij}	Strain tensor $= \left(\frac{\partial \bar{U}_i}{\partial x_j} + \frac{\partial \bar{U}_j}{\partial x_i}\right)$
$\bar{U}$	Mean velocity component in x direction
u	Fluctuating velocity component in x direction
$\bar{U}_i$	Mean velocity component in x_i direction
u_i	Fluctuating velocity component in x_i direction
u_τ	Friction velocity = $\sqrt{\tau_w/\rho}$
v	Fluctuating velocity component in y direction
x, y	Coordinates
y	Wall distance
z	Axial coordinate
	Greek Symbols
γ	Surface roughness of test tube wall
δ_{ij}	Kronecker's delta
ε	Dissipation rate of k
φ	Nanoparticle volume concentration
μ	Dynamic viscosity
ν, ν_t	Molecular and turbulent kinematic eddy viscosities
ρ	Density
σ_k, σ_ε	Turbulent model constants for diffusion of k and ε
τ, τ_w	Time and wall stress tensor
$\overline{(\,)}$	Time mean value
	Subscripts
bf	Base fluid
i, j, k	Index refers to spatial coordinates
nf	Nanofluid
P	Particles
t	Turbulent
w	Wall
	Superscripts
	Normalization by wall variables, i.e.,